


## PAPER

View Article Online  
View Journal | View Issue

Cite this: *Biomater. Sci.*, 2022, **10**, 4933

# Antimicrobial activity of piezoelectric polymer: piezoelectricity as the reason for damaging bacterial membrane†

Lea Gazvoda,<sup>a,b</sup> Milica Perišić Nanut,<sup>c</sup> Matjaž Spreitzer <sup>a</sup> and Marija Vukomanović <sup>\*a</sup>

Cell stimulation using piezoelectric polymers, which is known as piezostimulation, is an innovative approach for designing antimicrobial protection. As an antibiotic-free and inorganic nanoparticle-free approach, it uses physical stimuli to target bacterial cells in a non-specific manner, which may be of great importance, particularly in the context of avoiding resistant bacterial strains. In this study, we prepared fully organic piezoelectric biodegradable films composed of poly-L-lactide (PLLA) and demonstrated their antimicrobial effect on *S. epidermidis* as a model of Gram-positive and *E. coli* as a model of Gram-negative bacteria. The PLLA films were either smooth and fabricated using simple melt-drawing or nanotextured, as self-standing nanotubes formed using the template-assisted method. The morphological differences between nanotextured and smooth films resulted in a larger surface area and better surface contact in nanotextured films, together with improved structural properties and better crystallinity, which were the main reasons for their better piezoelectric properties, and consequently stronger bactericidal effect. The comparison between the nanotextured surfaces with and without piezoelectric nature excluded the main role of morphology and directly confirmed piezoelectricity as the main reason for the observed antimicrobial effect. We also confirmed that piezo-stimulation using the antibacterial nanotextured film could damage the bacterial membrane as the main mechanism of action, while the contribution of pH changes and ROS generation was negligible. More importantly, the effect was selective toward the bacterial membrane and the same damage was not observed in human red blood cells, making the therapeutic use of these films possible.

Received 26th April 2022,

Accepted 4th July 2022

DOI: 10.1039/d2bm00644h

rsc.li/biomaterials-science

## Introduction

Physical stimuli (mechanical, magnetic, and electrical) affect bacteria cells in different, non-specific manners in comparison to biochemical stimuli (*i.e.*, antibiotics), presenting an interesting treatment alternative.<sup>1</sup> Given that physical forces keep the structure of a cell together, targeting the structure of the cellular envelope is a common mechanism of action. Piezo-stimulation implies the application of a charge, which accumulates at the surface of mechanically deformed materials, thus affecting the potential in the cell envelope. It contributes to disassembling and destroying the bacterial cell envelope, thus achieving an antimicrobial effect. Accordingly, as antibiotic-free and inorganic nanoparticle-free approach,

the main benefit of providing an antimicrobial effect using piezo-stimulation is the limited ability of bacteria to develop resistance to it. Piezo-stimulation is mostly investigated for stimulating mammalian cell growth and its contribution to faster wound healing.<sup>2–5</sup> However, optimizing piezo-stimulation for achieving bacterial cell death is important given that it can be effectively used in preventing acute and chronic wound infections and decreasing the application of antibiotics during post-surgical and post-traumatic recovery.

In comparison to electrostimulation, which uses a similar mechanism, piezo-stimulation has self-powering activation (produces charge simultaneously upon mechanical deformation) and does not rely on external electrical sources and application of electrodes. Furthermore, the advantages of fully organic piezoelectrics, including biocompatibility, biodegradability and simple processing, are the main reasons for the use of poly-L-lactic acid (PLLA) in their design. This polymer has a similar left-handed helix orientation as the natural piezoelectrics in the human body (collagen, chitin, and elastin<sup>6</sup>). It is characterized with shear mode piezoelectricity and an electric dipole component distributed throughout the molecule.

<sup>a</sup>Advanced materials Department, Jožef Stefan Institute, Ljubljana, Slovenia.

E-mail: marija.vukomanovic@ijs.si

<sup>b</sup>Jožef Stefan International Postgraduate School, Ljubljana, Slovenia

<sup>c</sup>Department of Biotechnology, Jožef Stefan Institute, Ljubljana, Slovenia

†Electronic supplementary information (ESI) available. See DOI: <https://doi.org/10.1039/d2bm00644h>


Twisting of the polymer film leads to the orientation of molecular dipoles and generation of an electrical charge,<sup>7</sup> which can provide an antimicrobial effect.

However, to date, the antimicrobial properties of fully organic piezoelectrics are very poorly explained, and consequently ineffectively exploited. In general, it has been proposed that piezoelectric materials can affect bacteria through a variety of processes, such as transmembrane current-induced electroporation,<sup>8,9</sup> disruption of metabolic system/membrane potential,<sup>10</sup> positive surface charge<sup>10,11</sup> and generation of reactive oxygen species (ROS).<sup>12</sup> In contrast to inorganic piezoelectrics,<sup>12,13</sup> where ROS generation has been experimentally detected and associated with the antimicrobial activity observed mainly at the cationic Poles, the investigation of the electrical effect of piezoelectric polymers (such as PLLA<sup>7,8</sup> and polyvinylidene fluoride (PVDF)<sup>10,13,14</sup>) in bacteria is in its infancy. Ando *et al.* suggested that three different mechanisms are responsible for the antibacterial effect for PLLA (electroporation due to high-voltage output, electric current and less likely ROS), which lead to the formation of pores through which the bacterial contents leak, thus killing bacteria.<sup>7</sup> In contrast to piezoceramics, polymeric piezoelectrics such as PLLA or PVDF do not possess sufficient piezoelectric properties ( $d_{33} > 100 \text{ pC N}^{-1}$ ) to hydrolyse water into ROS products, using ultrasound as a source of mechanical deformation.<sup>15</sup> Therefore, achieving antibacterial properties due to the production of ROS is less likely to be the mechanism. In the case of ultrasound-stimulated piezoelectric PVDF films, different effects have been observed, including bacterial proliferation/growth inhibition and adhesion/antifouling on both the positive and negative poled sides depending on the applied ultrasound frequency (4 or 40 Hz) used for film deformation. The surface charge (under static condition, without ultrasound) resulted in antifouling at cationic and adhesion at anionic pole. The damaging effect of the positive surface charge was detected in Gram-positive *S. epidermidis* and Gram-negative *E. coli* bacteria.<sup>10,16,17</sup> However, a systematic approach for the investigation of bacterial piezo-stimulation using PLLA films is still lacking in the literature. Particularly this type of investigation is needed due to the difference in deformation required for achieving polarization in these two polymers, *i.e.*, shear in PLLA and compression/stretching in PVDF.

The topological and morphological characteristics of surface of films are other factors contributing to antimicrobial effects. Some findings suggest that films prepared with nanotextured patterns on their surface, which initially have no antibacterial properties, exhibit a damaging effect on bacterial cells by mimicking the natural defence mechanism observed in cicada wings.<sup>18–21</sup> Due to the physical topography movements, the cell walls of the attached bacteria stretch and disfigure when they are in contact with the film, leading to cell rupture and death.<sup>19</sup> It has been observed that piezoelectric PLLA films with a nanotextured surface affect mammalian cells and promote their attachment during piezo-stimulation.<sup>22</sup> However, the effects of these films combining nano-

texturing and piezoelectricity on bacterial cells still remains unexplored.

Considering the above-mentioned description, the main goal of this work was finding clear evidence correlating the piezoelectricity of fully organic PLLA films with their antimicrobial effect and optimizing the film design toward higher bactericidal efficacy and better compatibility in mammalian cells. Accordingly, the antimicrobial properties of piezoelectric and non-piezoelectric PLLA films with smooth and nanotextured surfaces were evaluated for (i) their impact on ROS formation, (ii) the impact of their topography, and (iii) direct influence of charge generated due to piezoelectricity. The piezo-stimulation resulting in the bactericidal nature of their effect was confirmed in both Gram-positive and Gram-negative bacterial strains and the selectivity was examined in blood cells.

## Materials and methods

### Materials

Chemicals and materials used during the experiments: poly-L-lactic acid polymer L207 S (PLLA, Evonik, Germany); poly(D,L-lactide-co-glycolide) RG-505, 50 : 50 (P(DL)LA, Evonik, Germany); piezoelectric polyvinylidene difluoride metallised film (PVDF, Goodfellow, Germany); anodised aluminium oxide plates on aluminium substrate with  $200 \text{ nm} \times 30 \mu\text{m}$  pores (AAO, Topmembranes, China); methylene Blue (MB, Alfa Aesar, Germany); hydrochloric acid, HCl (J.T. Baker, Poland); hydrogen peroxide solution 30% (Carlo Erba Reagents, Germany); copper(II) chloride,  $\text{CuCl}_2 \cdot 2\text{H}_2\text{O}$  (Riedel-de Haën AG, Seelze-Hannover, Germany); orthophosphoric acid 85% (VWR Chemicals BDH, France); sodium chloride, NaCl (Carlo Erba Reagents, Germany); HEPES (Fisher Scientific, Taiwan); Luria/Miller Broth (LB, Carl Roth, Germany); agar (Fluka, Spain); glutaraldehyde solution 25% in  $\text{H}_2\text{O}$  (Sigma-Aldrich, Co., USA); bacterial strains *Escherichia coli* (*E. coli*, ATCC 47076) and *Staphylococcus epidermidis* (*S. epidermidis*, ATCC 12228); labelling dye FM<sup>TM</sup> 4-64 (*N*-(3-triethylammoniumpropyl)-4-(6-(4-(diethylamino)phenyl)hexatrienyl)pyridinium dibromide, Invitrogen, Thermo Fisher Scientific, USA); DAPI (diamidino-2-phenylindole, Biotium, Fremont, CA) in Hank's balanced salt solution (Invitrogen, Thermo Fisher Scientific, USA); Live/Dead BacLight Bacterial Viability kit (L7007, Molecular Probes, Life Technologies, USA) and PrestoBlue<sup>TM</sup> Cell Viability Reagent (PB, Invitrogen by Thermo Fisher Scientific, USA). In all cases MilliQ (Purelab Option-Q, Elga) pure water was used.

### Film fabrication

Piezoelectric films were prepared using two approaches. Drawn films (DR) were prepared using the same conditions for stretching presented in our previous work.<sup>23</sup> Briefly, the polymer was hot-pressed above its melting temperature ( $250^\circ\text{C}$ ) into amorphous films and quenched in a cold water bath (DR1). These films were cut into a dumbbell shape and



clamped in a drawing machine, stretched at 80 °C to a draw ratio of 5 (DR5) at a speed of 40 mm min<sup>-1</sup>. Nanotextured films (NT) were prepared using a one-side-closed AAO porous template on an aluminium substrate, containing pores with a size of 200 nm thick and 30 µm long. The preparation route was similar to that for the previously reported films by Smith *et al.*<sup>24</sup> The was melted on glass covered with aluminium foil at 250 °C using a magnetic stirrer with hot plate (MSH-20D). After, the AAO template with open pore side was lowered on the polymer melt and pressed using a 1 kg weight and left to fill for 2–3 min. Subsequently, the films were removed from the heater and left to cool (NT as-prepared). To achieve improved crystallinity, the whole polymer inside the AAO template was annealed in a furnace at 160 °C for 1 h and left to cool slowly (NT ANN). The template was removed in 3 steps according to the manufacturer's instructions with slight modification. The back closed side of AAO was removed by immersing the film in 40% orthophosphoric acid for 6 h, and then the aluminium capping was etched using CuCl<sub>2</sub>·2H<sub>2</sub>O/HCl (4%/2%) solution overnight, and then transferred again to 40% orthophosphoric acid to remove the aluminium oxide pore walls in the membrane. After complete removal, self-standing nanotubes on the excess polymer substrate were left as a nanotextured film (NT). The obtained films were washed with water and ethanol and left to dry.

Extracted nanotubes were prepared with additional grinding of the excess of polymer filling before removing the template. When only filled pores remained in the template, membrane was removed with the same step explained above. Between steps, washing and changing the solutions were performed by centrifuging the samples in Eppendorf tubes at 12 500 rpm for 20 min. The nanotubes were washed with water at least 5 times and left in the wet state for further XRD and Raman analyses.

### Physicochemical characterization

A drop of the extracted nanotubes was dried on a silica substrate. Silica was used to enhance the signal of a small single nanotube. To estimate the orientation of the polymeric chains inside the single nanotube, Raman spectroscopy with polarized light was performed using an NTEGRA Spectra NT-MDT and polarised 488 nm laser source in the frequency range of 100–3200 cm<sup>-1</sup>. The acquisition was set to 100 s with a laser power of 5 mW, under which we did not observe signs of degradation. The results were labelled HHH and HVV, where the first letter corresponds to the fibre direction (horizontal), while the second and third are the orientation of the polariser and analyser (H-horizontal, V-vertical), respectively. All peaks were normalized to [0,1] relative to the silica main peak at 970 cm<sup>-1</sup>. For the orientation of the C–COO groups, the intensities were compared in the horizontal (HHH) and vertical (HVV) directions for the peak value at 875 cm<sup>-1</sup>. For the stretched samples, the observed peak intensities were normalized to the CH<sub>3</sub> asymmetric bending mode at 1454 cm<sup>-1</sup>. The orientation factor (*R*) was calculated as (HHH) *versus* (HVV) value for the C–COO peak.

Differential scanning calorimetry (DSC) analysis was performed using a NETZSCH STA 449 thermal analyser (Jupiter). Around 8 mg of sample was placed in platinum crucibles and heated in an Ar/O atmosphere (40/10) in the temperature range of 40 °C to 600 °C at a heating rate of 20 °C min<sup>-1</sup>. In the case of the nanotextured films, the excess polymer outside the AAO template was ground off to measure only the properties of the inner nanotube pores. The enthalpy of cold crystallization ( $\Delta H_c$ ) and enthalpy of melting ( $\Delta H_m$ ) were determined by calculating the surface under the peak of crystallization or melting, respectively. Bulk crystallinity was determined using the following expression:  $X_c (\%) = (\Delta H_m - \Delta H_c) / \Delta H_{(100\%)} \times 100\%$ , where the value for  $\Delta H_{100\%}$  was taken as 93.6 J g<sup>-1</sup>, which is the theoretical value for 100% crystalline PLLA films in the  $\alpha$ -crystalline form.<sup>25</sup> The weight fraction of polymer in the sample was calculated using thermogravimetric (TG) analysis and used for correction of the measured enthalpy initially normalized to the weight of the whole sample.

X-ray diffraction (XRD) analysis was performed on a BRUKER AXS D4 ENDEAVOR (Cu K $\alpha$  radiation ( $\lambda = 1.54$  Å),  $2\theta$  range 10°–40°, 0.04° step size with 5 s capture time) and EMPYREAN ( $2\theta$  range 15°–18°, 0.026° step size with 400 s capture time) to confirm the crystallinity of the prepared films and nanotubes. To perform measurements on the films, the edges of the samples were taped to the surface of the holder. For the extracted nanotubes, a suspension was added to a monocrystalline holder and the XRD patterns were measured focusing on the  $2\theta$  peak at around 16.5°.

The morphology of the polymer films was investigated using a scanning electron microscope (SEM-JSM 7600F, Jeol). For SEM microscopy, the samples were sputtered with gold using a BAL-TEC SCD sputter coater to prevent charging on the surface. The samples were observed under a low voltage (5 kV).

The wetting angle was measured using a Theta Lite-Biolin, Scientific contact angle meter. To determine the hydrophilic properties of the surface of the polymer films, a 5 µL drop of distilled water was used. The results are presented in the ESI.†

### Direct and indirect voltage output measurements

**Direct voltage output measurement.** The voltage output was measured when the films were subjected to mechanical stimulus using an ultrasonic bath (Elmasonic P, Elma, Germany). The films were sputtered with gold, acting as electrodes on both sides and connected to cables. The cables were attached to the electrodes using a protective adhesive polyimide film (3M, USA) on both sides with extremely low electrostatic discharge properties, which covered the sample. The edges were coated with nail Polish to ensure sealing against water intrusion during measurement. After impregnation against water intrusion the samples were placed in the US bath and stimulated at 37 kHz or 80 kHz. We used the listed frequencies according to the ultrasonic bath device settings due to the simplicity and usability of the system to mechanically stimulate the samples. Cables was routed through the piezo-film to a Kaysight MSOX3034T oscilloscope to record the signal.



**Indirect voltage output measurements (ROS generation potential).** A stock solution of methylene blue (MB) ( $1 \text{ mg mL}^{-1}$ ) was prepared in MilliQ clean water and kept in the dark for further use. The films were washed in water, placed in a 1:1 V/V mixture of MB and water ( $0.5 \text{ mg mL}^{-1}$ ) with or without 5% of peroxide ( $0.5 \text{ M H}_2\text{O}_2$ ) and sonicated with 37 kHz or 80 kHz ultrasound during the measurement. During the testing, all the samples (piezoelectric films DR5 and NT ANN and as-prepared films, PVDF as the working reference, and non-piezoelectric films NT P(DL)LA and DR1) were protected from light using amber 15 mL tubes. Every 20 min, 100  $\mu\text{L}$  aliquots were transferred on a transparent 96-well plate for absorbance measurement at 665 nm on a microplate reader (H1 Hybrid Multi-mode Microplate Reader, Synergy). Degradation was calculated as follows:

$$\text{Degradation (\%)} = 100\% - \left( \frac{(A_{\text{time}} - A_{\text{empty}})}{(A_{\text{initial}} - A_{\text{empty}})} \times 100\% \right)$$

All samples were tested in duplicate and for each, the absorbance was measured twice.

### Antibacterial testing

**Susceptibility tests during piezostimulation.** Gram-negative (*E. coli*) and Gram-positive (*S. epidermidis*) bacteria were tested in saline (0.9% NaCl) and Luria-Bertani (LB) growth medium to observe the effect of the piezoelectric film and ultrasonic piezo-stimulation on bacteria. In saline solution, an  $\sim 10^8 \text{ CFU mL}^{-1}$  (OD 0.1 for *E. coli* and OD 1 for *S. epidermidis*) stock suspension was used for testing in suspension or following the ISO22196 standard for testing the antimicrobial properties of the non-porous and non-absorbing surfaces.<sup>26,27</sup> To prepare bacteria in saline solution, bacteria were centrifuged (6000 rpm, 5 min) and the growth medium was discarded and replaced with saline solution. Prior to all antimicrobial assays, the films were sprayed with 70% ethanol solution and allowed to dry under laminar flow for sterilization. The films ( $0.5 \text{ cm} \times 1 \text{ cm}$ ) were immersed in the bacteria suspension and stimulated using an ultrasonic bath for 30 min using 80 kHz frequency. After sonication (US), the samples were incubated at 37 °C, while gently shaking using a MAX Q 4000 (Thermo Scientific) shaker. For bacteria counting, the sample solution was further diluted and drop-casted (10  $\mu\text{L}$ ) in triplicate on solid agar plates for counting. The plates were incubated overnight in a bacterial incubator (Kambič I-105 CK UV) at 37 °C before counting. The adjusted drop test (following the ISO22196 standard) was performed to observe the bacteria in full contact with the film, tested in saline solution (NaCl), where a 15  $\mu\text{L}$  drop was placed inside the wells of a 24-well plate and covered with the prepared films. After US stimulation of the plate, the samples were incubated at 37 °C, while maintaining high humidity, and thus no water evaporated from the drop. After 24 h, the films were washed with saline solution (500  $\mu\text{L}$ ) and dilutions was placed on solid LB agar plates for counting. Part of the film with attached bacteria was put in LB growth medium (200  $\mu\text{L}$ ) in a 96-well plate and Presto blue

indicator (5%) added to observe if any surviving and viable bacteria remained. Part of the washed bacteria solution was also transferred to a plate with added LB growth medium (1:1) and Presto blue indicator added to confirm if any remaining viable bacteria were left. For testing the kinetics in growth medium (LB),  $10^5 \text{ CFU mL}^{-1}$  bacteria stock solution was prepared. The films ( $0.5 \text{ cm} \times 1 \text{ cm}$ ) were placed upright in 200  $\mu\text{L}$  bacteria suspension on a 96-well plate in triplicate and incubated in a microplate reader (H1 Hybrid Multi-mode Microplate Reader, Synergy) to follow the growth curve by measuring the absorbance at 600 nm (OD600) for 20 h. Live/dead testing was performed according to the manufacturer's instructions. A 20  $\mu\text{L}$  drop of a dye mixture (propidium iodide (PI) and Syto 9) was put on the film and observed under a fluorescence inverted microscope (Nikon Eclipse Ti-U inverted microscope).

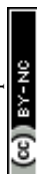
**Observing ROS effect during piezostimulation.** Sterile films were immersed in saline solution with bacteria ( $\sim 10^8 \text{ CFU mL}^{-1}$ ) in a 2 mL Eppendorf tube. A 20 $\times$  diluted stock solution of ascorbic acid ( $0.7 \text{ mg mL}^{-1}$ ) was added to each well as an antioxidant to prevent any possible ROS to disturb the bacteria. After 30 min of sonication followed by 24 h of incubation, the diluted bacteria were spread on agar plates and grown for an additional 24 h at 37 °C for counting colonies.

**SEM morphology in piezo-stimulated bacteria.** Samples containing bacteria were fixed in 2 wt% aqueous solution of glutaraldehyde for 1 h and washed with saline solution. This was followed by a dehydration step to exchange the water inside the cells with ethanol. For this, the samples were subsequently immersed in series of ethanol solutions (30%, 50%, 70%, 90% and 3 $\times$  100% EtOH) and incubated for 15–30 min in each of them. In the final phase, the samples in ethanol were dried under  $\text{CO}_2$  critical conditions using a critical point dryer (K850, Quorum Technologies). The dry samples were coated with a 10–15 nm gold layer and analysed using a JEOL JSM-7600F SEM.

**Bacterial membrane integrity after piezostimulation.** After piezostimulation of the bacteria with the films and incubation for 24 h, 100  $\mu\text{L}$  was centrifuged for 5 min at 6000 rpm, and the supernatant was replaced with 50  $\mu\text{L}$  of FM 4-64/DAPI containing 0.4  $\mu\text{L}$  of 5  $\text{mg mL}^{-1}$  (FM 4-64 and 1  $\mu\text{L}$  of 125 $\times$  DAPI). After a short staining period, the bacteria were visualized with an LSM-710 confocal microscope (Carl Zeiss, Germany) equipped with UV (405 nm), Argon (488 nm and 514 nm), and HeNe (543 nm and 633 nm) lasers under 63 $\times$  magnification. The images were acquired and processed using the ZEN software (Carl Zeiss).

### Influence on red blood cells (hemolysis)

**Hemolysis after piezostimulation.** Films was incubated with red blood cells (RBC) using the same piezostimulation conditions as that for bacteria (80 kHz) with 100% and 30% power. For this, RBCs were diluted in 20 mM HEPES/0.9% NaCl buffer to 2.5% cells  $\text{mL}^{-1}$ . The films were immersed in 300  $\mu\text{L}$  prepared RBC solution in Eppendorf tubes and sonicated in an ultrasonic bath at 80 kHz for 30 min. After piezosti-





mulation, the films and RBCs were incubated at 37 °C for 4 h. Hemolysis was measured as absorbance reading at 540 nm for the supernatant after centrifugation (800 rcf, 5 min), using RBC in water as the positive control and non-treated RBC in HEPES/NaCl as the negative control.

**RBC membrane integrity after piezostimulation.** Staining of the membrane in RBC was performed following the same protocol as that for the bacteria using FM 4-64/DAPI fluorescent dyes.

### Statistical analysis

Data are expressed as mean  $\pm$  SD of one or two experiments performed in duplicate or triplicate. All graphs were plotted using OriginPro or GraphPad Prism. Statistical analysis was done using the GraphPad Prism software and standard one-way ANOVA test (a  $p$  value of  $<0.05$  was considered statistically different).

## Results and discussion

### Structural properties of PLLA nanotextured films

Herein, we present the difference in morphological and piezoelectric properties of PLLA polymer films prepared in nanotextured (NT) or smooth (DR) form, focusing on the impact of these films on Gram-negative and Gram-positive bacteria and their selectivity. Fig. 1 illustrates the process for the preparation of the piezoelectric NT or smooth drawn (DR5) films and the non-piezoelectric reference samples of NT P(DL)LA and smooth non-drawn (DR1) film, respectively, and their predicted behavior under ultrasound (US) and towards bacteria and blood cells (RBC).

Initially, the prepared films were morphologically and structurally analysed to determine their crystallinity and orientation properties required to execute a piezoelectric effect.

**Morphological study of prepared films.** The organic films formed using PLLA (with more than 90% L-lactic acid stereo-

isomer) and produced by mechanical drawing (DR5) (Fig. 2(a)) and using a porous template (NT ANN) (Fig. 2(b)) exhibited a significantly different surface morphology. The PLLA DR5 films had a rough surface with respect to the non-drawn films, but flat with respect to the NT films, with amorphous clusters covering the oriented polymer chains in the drawing direction (Fig. 2(a)).

Alternatively, texturing (Fig. 2(b)) and tube formation (Fig. 2(c)) were confirmed by closely observing the surface of NT PLLA, where nanotubes were arranged in island-like groups on the polymer substrate at the bottom of the film (as indicated in Fig. 2(d)). The tubes on the surface of the annealed film possessed an average radius of  $177 \pm 28$  nm and length of  $27 \pm 2$   $\mu$ m (Fig. 2(c) and (d)), indicating the filling of the pores inside the templates during their formation to the top. The same approach was applied to produce the non-piezoelectric nanotextured film reference (NT P(DL)LA) using a copolymer with a 50 : 50 ratio of poly(D,L-) lactide and poly-glycolide. The tubes on the surface of P(DL)LA possessed a diameter of  $167$  nm  $\pm$  24 nm (ESI S1 (Fig. S1<sup>†</sup>)), confirming their similar morphology to that of NT PLLA.

**Crystallinity and crystal structure.** The combination of high crystallinity and directional polymer backbone chain orientation is desirable to exploit the shear piezoelectric properties of the PLLA polymer,<sup>28</sup> and therefore these properties were investigated initially.

Additional processing of the NT and DR films improved their crystallinity, as observed in their XRD (Fig. 3(a and b)) and DSC (Fig. 3(c and d)) patterns, respectively. After applying stretching and the formation of DR5, strain-induced crystallization occurred, which resulted in (110)/(200)-oriented crystalline regions in their  $\alpha$ -crystalline structure. In comparison to these films, the non-drawn films (DR1) were amorphous. Applying annealing induced crystallization, as observed in the case of the DR1 films annealed above 140 °C. In this case, the non-oriented and annealed film (DR1 ANN) showed high crystallinity with additional orientations of crystalline regions

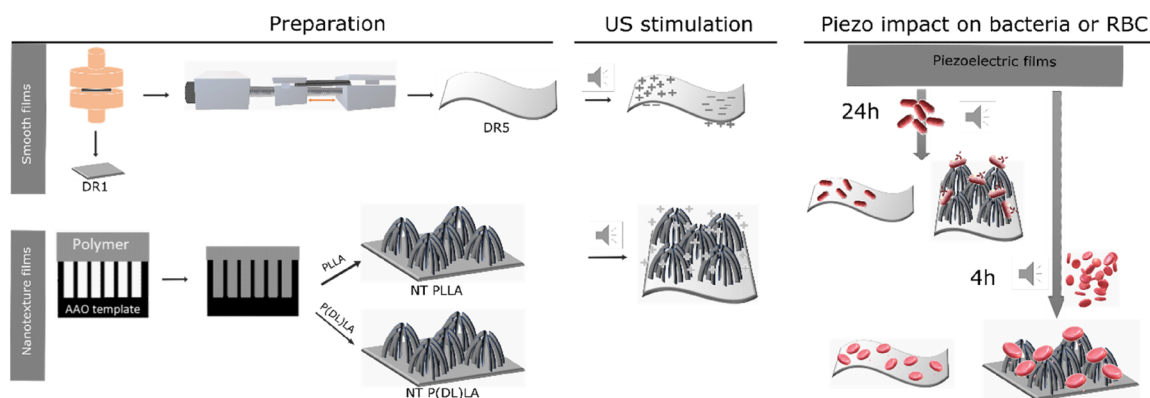


**Fig. 1** Schematic presentation of the preparation of smooth piezoelectric (DR5) and non-piezoelectric (DR1) and nanotextured piezoelectric (NT PLLA) and non-piezoelectric (NT P(DL)LA) polymer films and their expected response to ultrasound stimuli as generation of positive charge on the stretched upper side of the down bent polymer and negative charge on the bottom bent side; and piezo-stimulated damaging impact on bacteria for nanotextured film and not harmful behaviour towards RBCs.



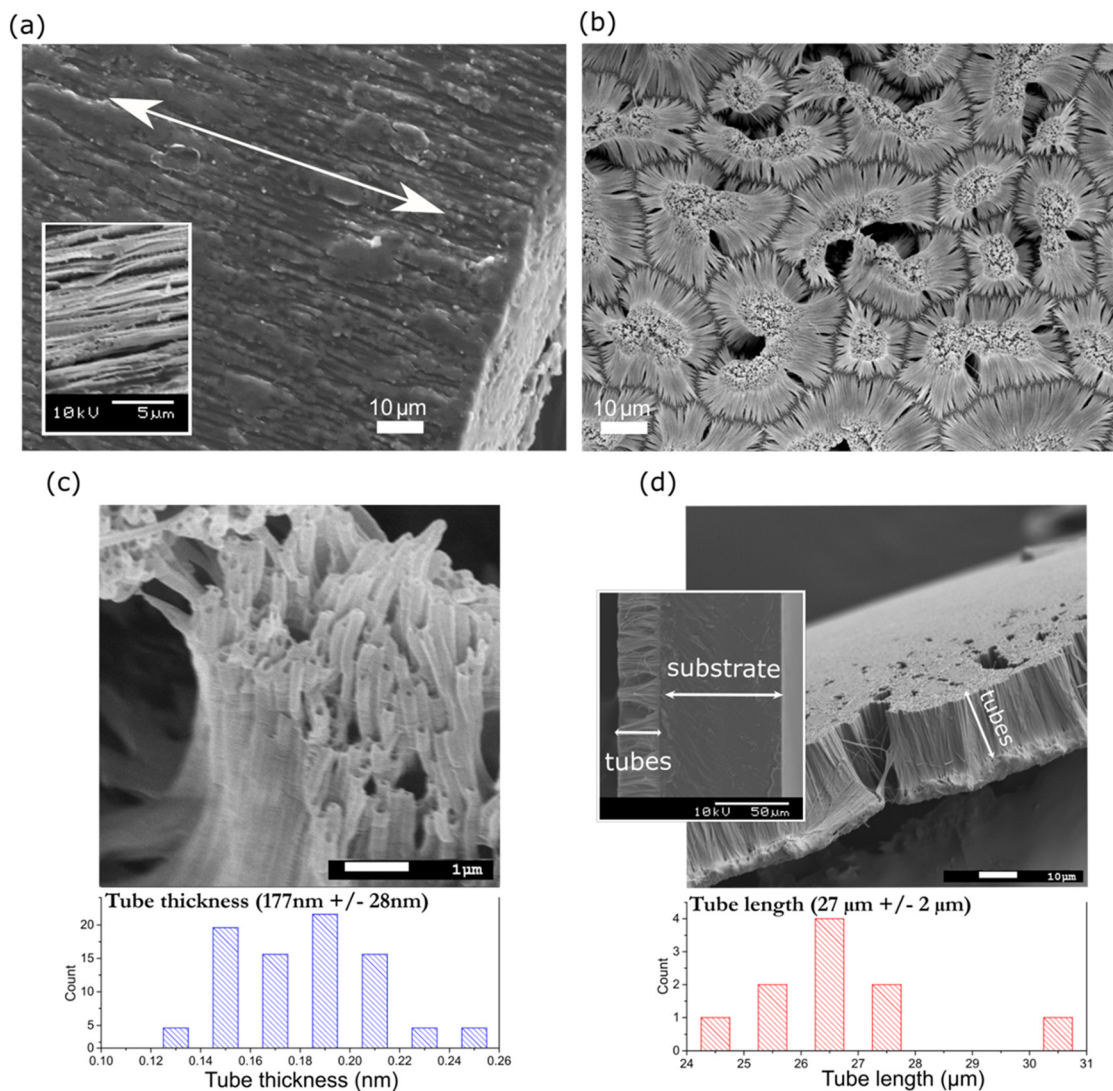


**Fig. 2** Scanning electron microscopy analysis of (a) drawn film with a draw ratio of 5 (DR5) with arrow presenting the drawing direction and image of the cross-section in the white square, (b) surface of nanotextured annealed film (NT ANN), where tubes tend to form lean to island-like groups, (c) closer look of NT ANN film, confirming the formation of tubes and (d) cross-section to determine tube length from polished polymer substrate and image of actual prepared film in white square, and (c) and (d) show size distribution histograms of average tube thickness and length, respectively.

present in the  $\alpha$ -crystalline structure, as identified based on.<sup>29</sup> The DR5 film was crystalline; however, due to the presence of a cold crystallinity peak, there is still room for improvement, and therefore after annealing, full crystalline potential was achieved (DR5 ANN), as observed by DSC (Fig. 3(c)).

The as-prepared NT film also possessed an amorphous structure (Fig. 3(a)). It crystallized only after annealing, with the appearance of the (110)/(200) crystalline peak. The position of this peak shifted to lower  $2\theta$  values compared to that of the smooth film, indicating the formation of a more disordered  $\alpha'$ -crystalline structure. When the same approach was applied for the formation of the NT P(DL)LA film, even after annealing its structure remained amorphous.<sup>30</sup> For the non-drawn copolymer P(DL)LA film, the DSC results showed only an amorphous peak and lack of melting peak, indicating that the polymer

could not crystallize at temperatures up to 200 °C (Fig. 3(c)). Therefore, this polymer was used as a non-piezoelectric reference in the case of the NT-prepared films.

It should be considered that for the NT films, nanotubes were formed on the substrate (bottom part of the film), which held them at their surface (as indicated in Fig. 2(d)). Given that the bottom part was thicker than the nanotubes, most of the XRD signals for the film come from the substrate. This is the reason why the nanotubes were extracted from the substrate and the XRD pattern of only the nanotubes was recorded (Fig. 3(b)). The results show that the as-prepared nanotubes had low crystallinity, while after annealing for 1 h at 160 °C, their crystallinity improved and shifted to the  $\alpha'$ -crystal form. Considering that both the  $\alpha$  and  $\alpha'$  PLLA structures possess piezoelectric properties<sup>23</sup> due to the helix structure of the



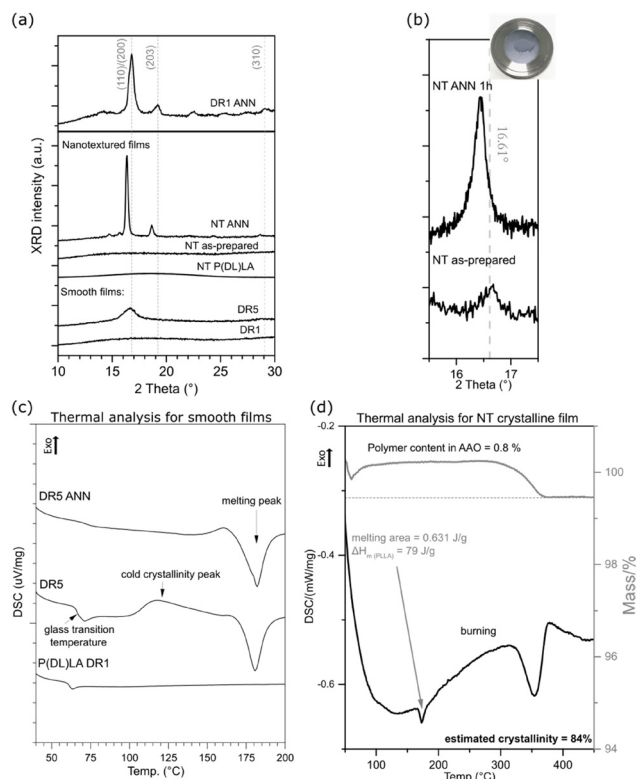


**Fig. 3** (a) XRD diffractograms of nanotextured films (NT as-prepared, annealed (NT ANN) at 160 °C for 1 h and for P(DL)LA as-prepared (NT P(DL)LA)) and smooth films (non-drawn (DR1) and drawn (DR5)) compared to unoriented annealed film (DR1 ANN) at 160 °C for 1 h. (b) XRD of mechanically extracted nanotubes for NT as-prepared and NT ANN tubes. Thermal analysis (DSC and mass lost) of (c) drawn films (DR5, DR5 ANN and P(DL)LA DR1) and (d) filled AAO template with polymer excess ground off on the bottom of the NT ANN sample.

polymer chain, annealing for 1 h was used for further analysis of the NT films with bacteria.

To quantify the crystallinity of the nanotubes, we applied thermal analysis and the DSC signal was measured for the AAO template with the polymer-filled pores and polymeric substrate removed (the substrate, as indicated in Fig. 2(d), was ground off). The DSC curve (Fig. 3(d)) does not show peaks corresponding to the cold crystallization and glass transition (which are properties of the low-ordered, amorphous phase), only a peak corresponding to melting, indicating an ordered structure with high crystallinity. We assumed that the entire peak area belongs to the polymer inside the pores, which represents only 0.8% of the mass of the whole sample. The estimated value was calculated to be around 84% crystallinity, which is extremely high compared to the smooth DR5 films, where upon annealing for 1 h, the maximum of 62% crystallinity was achieved.<sup>23</sup> Smith *et al.* measured 53% crystallinity for nanotube films prepared in a similar manner; however, they measured the whole film together with the substrate, meaning that most of the signal came from the larger bottom part.<sup>24</sup> Also, 70% crystallinity was obtained for PLLA fibres prepared from solution at 100 °C.<sup>31</sup> The DSC and XRD results also con-

firmed that annealing increased the crystallinity of the drawn films (DR5), and that P(DL)LA polymer only shows amorphous behaviour. The improved crystallinity after annealing of both the NT and DR films (detected by XRD and thermal analysis) indicates that this post-processing step also improved their piezoelectric properties.

**Orientation properties of films.** The chain orientation in the PLLA films was observed using Raman spectroscopy with polarized light. Due to the small dimensions of a single nanotube, its signal was enhanced using a silica substrate (Fig. 4(a)). The orientation of the thicker DR5 ANN film was also confirmed (Fig. 4(b)), where its intensities were higher. The intensities of the C-COO peak at 875 cm<sup>-1</sup> were obtained using different, horizontal and vertical, directions of light and compared. In both films, the fibres were in the horizontal position; therefore, the signals from two light-directions were assigned to nanotube stretching (HHH) and nanotube perpendicular direction (HV), which were used to calculate the nanotube orientation factor ( $R = I_{HHH}^n / I_{HV}^n$ ) (Fig. 5(c)). Using this approach, we confirmed that chain orientation in the nanotubes follows the longitudinal direction of the AAO pore, where they were formed ( $R = 1.31$ ). In the AAO template, the melted polymer solidifies on the surface of nanopore wall. Due to the rapid growth along these nanopores, the polymer chain orientation follows the pore direction. A similar mechanism of nanotube formation and orientation was previously observed for the PS-*b*-PLLA copolymer and PAO nanotubes,<sup>24,32</sup> Besides the single nanotubes, the polymer chain orientation was also confirmed for the drawn films (DR5). The orientation factor obtained for the drawn films ( $R = 2.45$ ) was distinctly different from that of the non-oriented annealed film ( $R = 0.80$ ). Similar to the nanotubes, the chain orientation in the drawn films followed the direction of drawing used for their formation. This implies that both the capillary forces, which stretched the polymer inside the nanotube template, and mechanical forces used for film drawing had the same role in the formation of their structures.

### Estimation of piezoelectric properties through piezo-degradation potential of organic dye

The films were mechanically deformed using US to measure their piezoelectric properties by measuring the voltage generated during their deformation. Using an ultrasonic bath, the direct voltage output was measured for the PLLA films and compared to the standard with known piezoelectric properties (PVDF film). According to Cafarelli *et al.*, US waves are mechanical waves that travel through the medium, and combined with US-responsive materials, US can be used for the stimulation of piezoelectric materials for the generation of a localized electric field due to the direct piezoelectric effect.<sup>33</sup> The effect of ultrasound on the film is dependent on the pressure it can produce through the cavitation of bubbles. Rashwan *et al.* explained that at a fixed intensity (in our case, the power of the ultrasonic bath was fixed), in a low ultrasonic frequency range (20–50 kHz), the difference between the minimum and maximum pressure is small compared to that





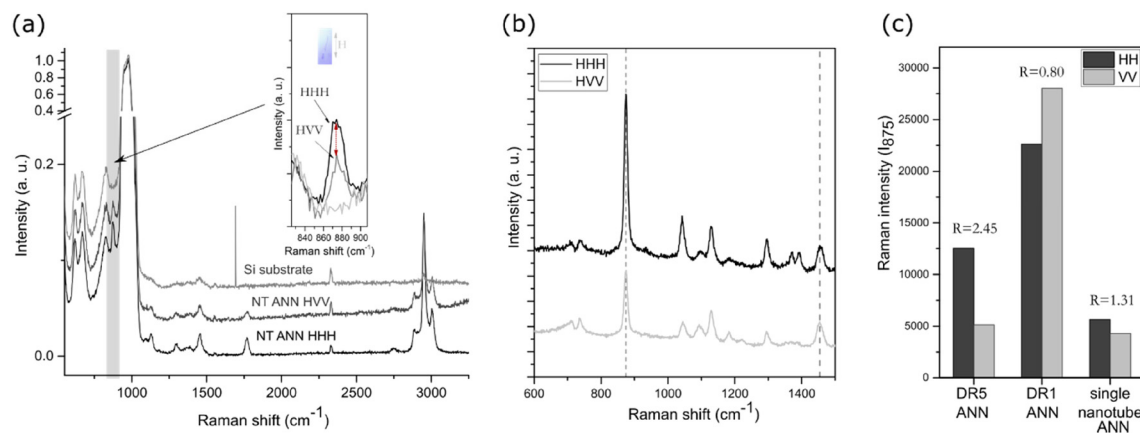


**Fig. 4** Polarized Raman spectra of (a) extracted annealed nanotubes in pore length direction (HHH) and perpendicular (HVV) for orientation assessment with magnification of 875 cm<sup>-1</sup> peak (b) and drawn film in drawing direction (HHH) and perpendicular (VVV). (c) Comparison of Raman intensities for horizontal and perpendicular values of 875 cm<sup>-1</sup> peak for annealed drawn film (DR5 ANN), non-oriented film (DR1 ANN) and single nanotube, with calculated orientation ratio ( $R$ ) as HHH normalized to VVV values.

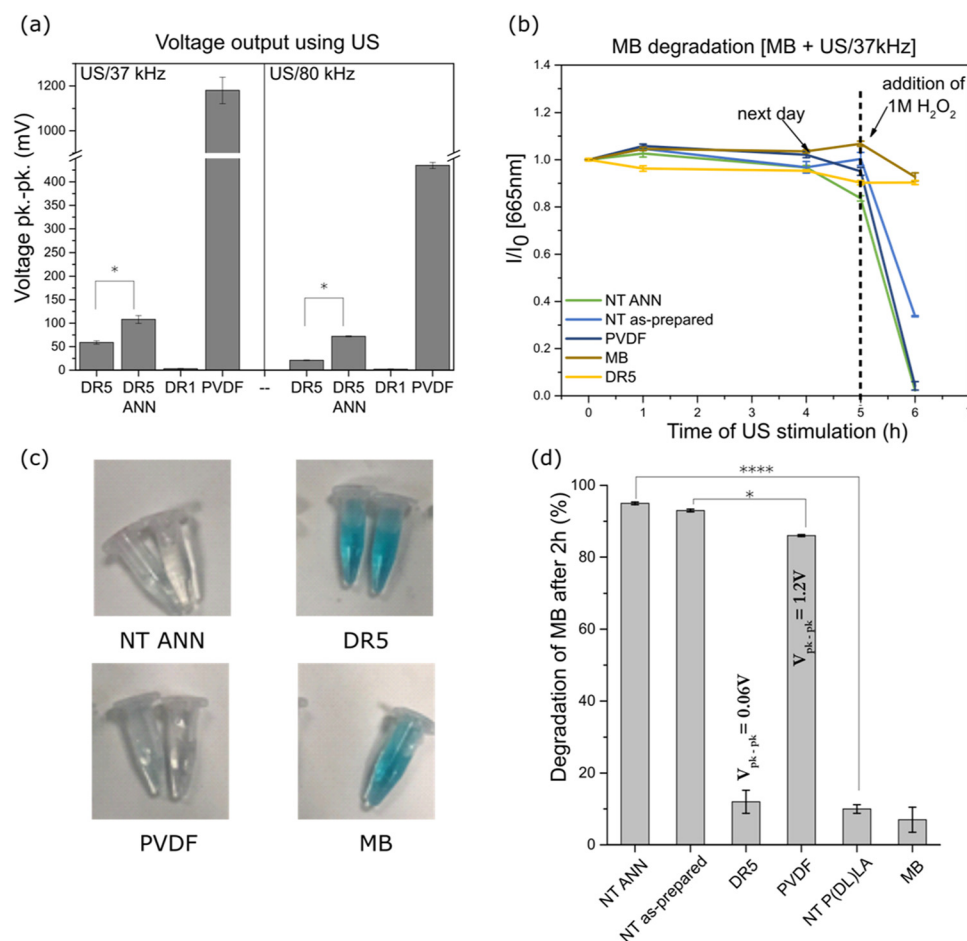


**Fig. 5** (a) Voltage peak-to-peak output data collected for US-stimulated piezoelectric films at 37 kHz and 80 kHz for drawn (DR5), drawn and annealed (DR5 ANN), non-drawn (DR1) and PVDF reference sample; (b) methylene blue (MB) degradation observed through absorbance measurements (665 nm) under 37 kHz ultrasound stimulation with marked addition of 1 M hydrogen peroxide (H<sub>2</sub>O<sub>2</sub>) for nanotextured annealed film (NT ANN), as-prepared nanotextured film (NT as-prepared), smooth drawn film (DR5) and reference sample of PVDF film and clear MB solution; (c) visual presentation of colour change after MB degradation for above-mentioned samples; and (d) percentage of MB degradation after 2 h of ultrasonication with 0.5 M hydrogen peroxide as active species in contact with the above-mentioned samples and for non-piezoelectric nanotextured film (NT P(DL)LA); where \* and \*\*\*\* annotate  $p < 0.05$  and  $p < 0.0001$ , respectively.





at higher frequencies (55–80 kHz) where it is much larger. A larger difference means that the periodic time of the wave cycle is reduced, and therefore bubbles take more time to grow before collapsing. At lower frequencies, more bubbles cavitate and are more powerful, consequently generating a higher pressure and temperature on the films compared to that at higher frequencies.<sup>34</sup> Given that the changes in cells occur due to the US stimulation of the piezoelectric PVDF (which requires transverse deformation)<sup>35</sup> and PLLA (requiring shear deformation)<sup>36</sup> polymer, we believe that the application of ultrasound can excite both transverse and shear piezoelectricity.

PVDF showed the highest peak-to-peak output voltage of 1.2 V (Fig. 5(a)) at 37 kHz and less than half this value at 80 kHz (450 mV). A similar trend was observed for the DR5 films and films that were additionally annealed. The values were much lower at 37 kHz compared to that of the PVDF reference (59 mV and 108 mV for DR5 and DR5 ANN, respectively), while at two-times higher frequency, they were around two-times lower. Given that annealing of the DR5 film improved its crystallinity; consequently, its piezoelectric properties were at least 2-times higher at both frequencies (Fig. 5(a)). A clear difference was observed between drawn (DR5) and non-drawn film (DR1), given that the shape of the curve differed from the noise, as presented in ESI S2 (Fig. S2†).

The same method was unsuitable for the NT films, given that the electrodes were difficult to adjust for the complex surface made of individual nanotubes. Therefore, we applied an indirect method to estimate their piezoelectric properties by measuring their piezo-degradation potential. We took advantage of the ability of hydrogen peroxide to catalytically decompose into reactive oxygen species (ROS), which degrade the organic dye methylene blue (MB). In this reaction, the piezoelectric film acts as the catalyst. As previously observed, the ROS formed by piezo-catalysed  $\text{H}_2\text{O}_2$  oxidation were responsible for the discolouration of MB.<sup>37,38</sup> Fig. 5(b) shows the effect of US stimulation of the films on MB degradation by measuring the absorbance at 665 nm, which is presented as the normalized absorbance to the initial value. Without that addition of  $\text{H}_2\text{O}_2$  and after 5 h of continuous US stimulation, no MB degradation was observed, confirming that the investigated polymers were not capable of producing ROS by themselves. ROS products originating from the hydrolysis of water are commonly obtained for ceramic materials with much higher piezoelectric properties.<sup>39–41</sup> However, with the addition of  $\text{H}_2\text{O}_2$  with a redox potential lower than that of water, the investigated polymers could catalyse ROS, which allowed insight into their piezo-degradation capacity. Therefore, when highly concentrated  $\text{H}_2\text{O}_2$  was added, the total degradation of MB is observed for the NT piezoelectric films (NT ANN and NT as-prepared) and PVDF reference as compared to the clear MB or DR5 film with low piezoelectricity, where degradation did not occur. The observed effect is illustrated in the photographs presented in Fig. 5(c), showing the partial or complete discolouration of MB solution at the end of the stimulating process for the different films. In

addition, for the controls, we observed that MB/peroxide was not degraded by ultrasound without the films and that the films did not degrade MB/peroxide until ultrasound was turned on (ESI S3 (Fig. S3†)). This is direct evidence that the observed degradation processes were driven by the charge form on the surface of the films during their deformation and a direct consequence of their piezoelectricity. After the addition of a lower concentration of  $\text{H}_2\text{O}_2$  (0.5 M) the degradation kinetics were slower (kinetic curves presented in ESI S4 (Fig. S4 and S5†), which clearly revealed the differences in piezo-degradation potential among the investigated films (Fig. 5(d)). The highest piezo-degradation potential was observed for the piezoelectric NT PLLA films with the highest rate of MB degradation (95%) among the piezoelectric films, including PVDF and DR5 (86% and 12%, respectively) (ESI S4 (Table S1†)). The clear contribution of the piezoelectricity to MB degradation was observed when the degradation by the piezoelectric NT PLLA films was compared that of the non-piezoelectric NT P(DL)LA films with the same morphology and surface area. Specifically, the degradation rate obtained for the drawn DR5 films was very slow and not significantly different compared to the non-treated MB or non-piezoelectric NT P(DL)LA film, which is due to their low piezoelectric effect and small available specific surface area.

For the thin films and films with complex a morphology of nanotexture on the surface, the piezoelectric coefficient was difficult to measure, and therefore it was confirmed through piezo-potential for organic dye degradation.

### Antibacterial properties

After the detailed characterization of the structural, morphological and piezoelectric properties of the developed films, they were further investigated for their capacity to affect bacterial cells. Particularly we were focused on the individual contributions of different factors including film surface morphology, piezoelectricity, and ROS generation as the possible source of the antimicrobial effect. The tests were performed using *E. coli* as the representative Gram-negative and *S. epidermidis* as the Gram-positive bacteria.

Both piezoelectric PLLA films (NT ANN and DR5) initially possessed greater hydrophobic properties with a contact angle of around  $110^\circ$ ; however, after wetting their surface, the contact angle decreased ( $70^\circ$  and  $45^\circ$  for DR5 and NT ANN sample, respectively), indicating the better wettability of the NT films (ESI S5 (Fig. S6†)). Hydrophobic properties can play an important role in assessing the antibacterial properties of the samples due to the poor contact of the bacteria with the film surface.

**Direct contact-based antibacterial effect.** The antibacterial drop test, which is one of the standard tests to evaluate the antibacterial properties of non-porous and non-absorbing surfaces, was performed to assess the bacterial susceptibility to piezo-stimulation.<sup>26,27</sup> This test was the optimal choice given that it provides the best contact between the investigated bacteria and surface of the film, given that none of the antimicrobial agents are expected to be released in the surround-



ing medium. When a drop of bacteria (containing  $10^6$  cfu  $\text{mL}^{-1}$  or  $10^8$  cfu  $\text{mL}^{-1}$  of *E. coli* or *S. epidermidis*, respectively) was put on the piezoelectric NT PLLA films (both as-prepared and ANN), followed by US deformation, all the bacteria were killed after 24 h and no further survival was detected (Fig. 6(a) and (b)). In the case of the NT ANN films, with the highest piezoelectricity based on piezo-degradation potential (Fig. 5(d)), the antibacterial effect was observed even without US stimulation. Smith *et al.* demonstrated that the adhesion and further growth of human dermal fibroblasts on the surface of NT PLLA mechanically deformed the film, exhibiting a piezoelectric effect on the cells.<sup>22</sup> We also predicted the same after loading the bacteria on the NT PLLA films. This small deformation was high enough to activate the piezoelectric effect, providing a complete bactericidal effect on both bacterial strains (with 6 log 10 and 8 log 10 cfu reduction) even without the application of US deformation. The same was not observed for the drawn DR5 films with a much lower piezoelectricity. To clearly confirm death of the bacteria on the NT PLLA film surface, the washed solution and the films from the assay were also placed in growth medium to observe the viability of any surviving bacteria by following the 24-hour kinetics of PB fluorescence at 37 °C, finally confirming their bactericidal effect (ESI S6 (Fig. S7–S9†)).

The washed films after the contact test showed a clean surface without bacteria and their piezo-degradation potential toward MB dye degradation in the presence of peroxide was still observed (60% lower degradation compared to initial), indicating the possible reuse of the film, as presented in ESI S6 (Fig. S10†).

**Influence of surface texturing on antibacterial properties.** Another possible source of antimicrobial activity observed in the NT PLLA films could be potentially associated with their

nanotextured morphology. A nanotextured morphology (in the case of short and tightly packed nanopillars<sup>20,42</sup>) can exhibit a bacteriocidal effect by itself.<sup>20,21</sup> This type of morphology can also exhibit superhydrophobicity towards liquids, resulting in an anti-fouling and self-cleaning effect<sup>43</sup> and consequently repelling the attachment of bacteria.<sup>19</sup> To evaluate the influence of the surface morphology on the bactericidal effect observed for the NT PLLA films, we compared the antimicrobial effect in piezoelectric PLLA and non-piezoelectric P(DL)LA with the same surface morphology. The CFU count between the US-treated *E. coli* and bacteria in contact with NT P(DL)LA was not statistically different, where no log reduction occurred for the non-piezoelectric nanotextured film (Fig. 6(a) black square). In the case of the non-piezoelectric NT P(DL)LA films, a killing effect was not observed, and therefore the effect of the surface morphology was discarded. It can be assigned to the formation of long nanotubes (27  $\mu\text{m}$  in length) without dense packing (Fig. 3). This type of morphology enables bacteria to attach to the nanotube sides rather than their top, which is where their nanotexture-associated antimicrobial effect occurs.<sup>20</sup> The comparison between NT P(DL)LA and PLLA directly confirmed that piezoelectricity is the main reason for the observed antimicrobial effect.

**Kinetics of antibacterial activity in saline solution and growth medium.** The kinetics of killing bacteria in saline solution and the growth curves for the bacteria suspended in growth medium were also measured for *E. coli* and *S. epidermidis* bacteria. When the films were immersed and left to float in the bacteria saline suspension (*E. coli*), the NT ANN samples, US stimulated, still showed a clear bactericidal effect (Fig. 7(a)). After incubation for 1 h, we observed that after there was no difference between the non-treated bacteria and bacteria incubated with the films; while after 5 h at least

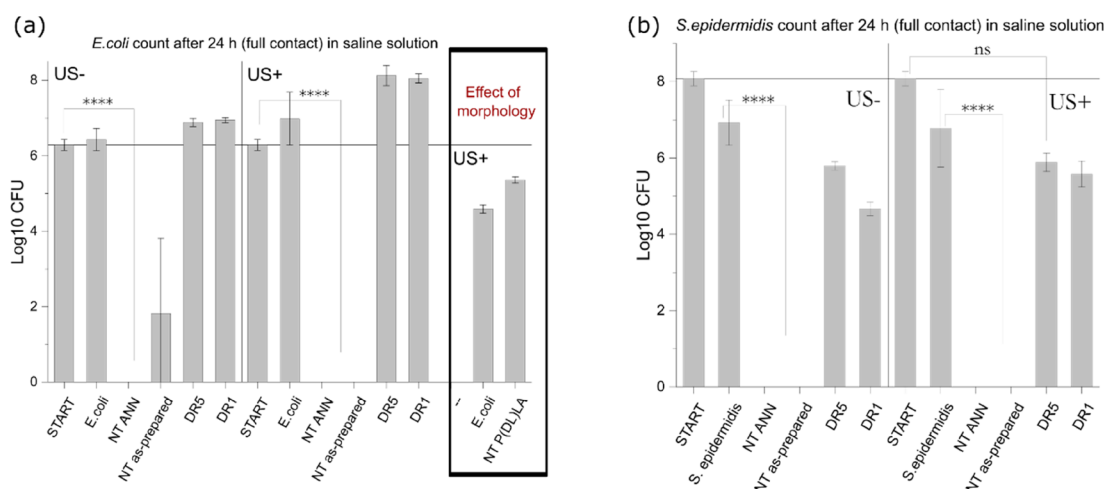


**Fig. 6** Full contact-based testing of PLLA films with *E. coli* bacteria. (a) Graph of counted CFU of surviving *E. coli* bacteria on agar plate, after contact with PLLA films (nanotextured annealed (NT ANN) and non-annealed (NT as-prepared), drawn (DR5) and non-drawn film (DR1)) with or without US stimulation for 30 min (annotated with US+ and US-); black square indicating separate contact test between *E. coli* and non-piezoelectric nanotextured film (NT P(DL)LA). (b) Graph of counted CFU of survived *S. epidermidis* bacteria in contact with above-mentioned films on agar plates after 22h of incubation; where \*\*\*\* annotates  $p < 0.0001$  and ns is statistically insignificant difference.



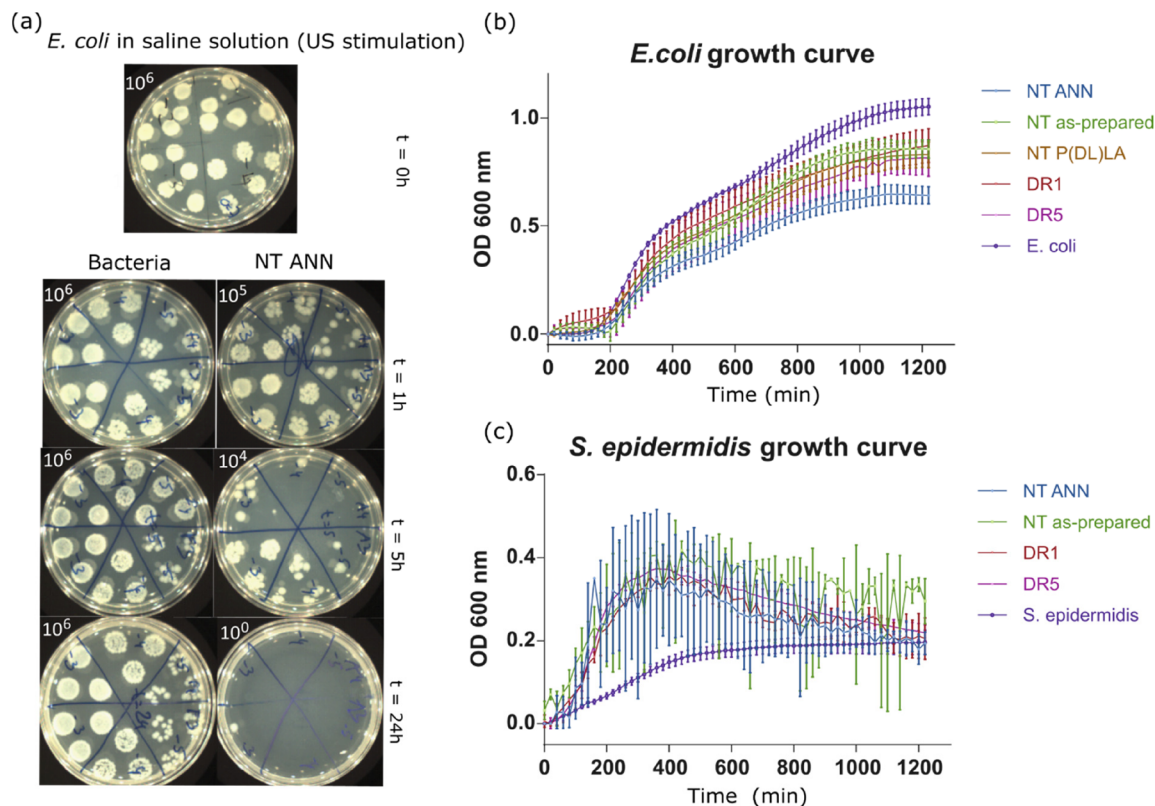


**Fig. 7** (a) Agar plates with diluted bacteria growth for *E. coli* and bacteria in contact with NT PLLA film at start and after 30 min US stimulation following 1 h, 5 h and 24 h incubation in saline solution. Kinetics of bacteria growth in LB medium after initial US stimulation for (b) *E. coli* bacteria and (c) *S. epidermidis* bacteria (presented only average values).

2 log 10 reduction was observed; and after 24 h, clear death resulting in 6 log 10 reduction was confirmed for the bacteria incubated with the immersed NT ANN film (Fig. 7(a)).

In the case when films were immersed in LB bacterial suspension, the differences in bacteria growth were insignificantly lower. In the case of both bacterial strains, *E. coli* (Fig. 7(b)) and *S. epidermidis* (Fig. 7(c)), the growth kinetic curves showed a small decrease in OD values, which was the most pronounced in the case of incubation with NT ANN films with *E. coli* bacteria (50%) (Fig. 7(b)). Testing in saline solution confirmed that killing bacteria using piezo-stimulation is not a fast process (>5 h). Therefore, if bacteria have the possibility to grow, such as in nutrition LB medium, the piezo-effect will not be pronounced or have a significant effect on bacteria growth. A similar small or no effect was also observed after stimulating bacteria with piezoelectric PVDF films in planktonic growth.<sup>10</sup> The hydrophobicity of the prepared samples can also be a reason for the insufficient film-bacteria contact, and therefore the observed poor antibacterial properties in growth medium solution.

**Influence of pH change and the effect of ROS.** Another aspect of the antimicrobial effect obtained for the US-deformed NT PLLA films can be associated with polymer degradation and generation of ROS. PLLA is a polyester, which degrades through hydrolysis, releasing acidic products and consequently decreasing the pH, particularly in the microenvi-

ronment close to the film surface. However this process is not fast, and as we observed earlier, degradation in the presence of enzymes takes several days.<sup>44</sup> This period is longer than the time needed for obtaining an antibacterial effect, and therefore the contribution of pH changes due to the release of lactic acid was discarded. More importantly, with polymer degradation, the piezoelectric properties gradually decrease,<sup>44</sup> implying the prolonged availability of their surface for providing piezo-stimulation-induced antimicrobial activity.

Alternatively, the generation of ROS is the main reason for the antibacterial effects obtained by strong piezoelectrics (such as piezoceramics).<sup>12</sup> This is ascribed to their capacity to hydrolyze water, as confirmed using the MB degradation test.<sup>39–41</sup> Using a similar MB test, we confirmed that none of the investigated PLLA and even PVDF reference did not have capacity for the degradation of MB in water (Fig. 5(b)). Consequently, ROS formation cannot be associated with the antimicrobial effect observed for NT PLLA. This was further confirmed with the addition of an ROS scavenger during antimicrobial testing. Specifically, we applied 0.035 mg mL<sup>-1</sup> ascorbic acid as a strong antioxidant to eliminate any potentially formed ROS during piezo-stimulation. Consequently, we did not observe any difference in bactericidal effect when bacteria were in contact with the NT-annealed films (Fig. 8(a)). This is clear proof that ROS were not responsible for killing the bacteria.



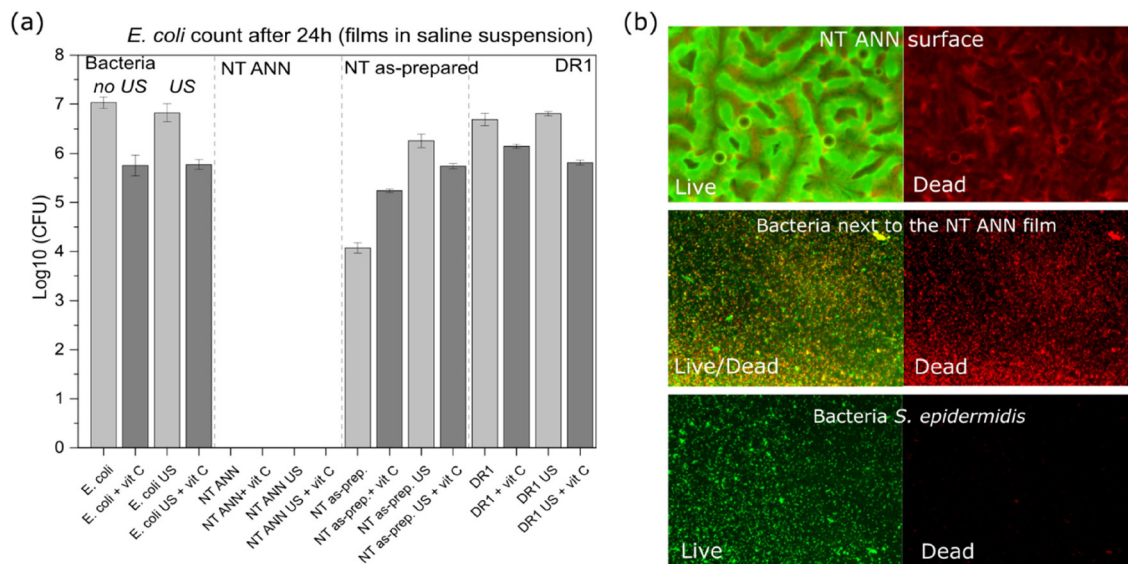


**Fig. 8** *E. coli* count of grown bacteria on agar plate after 24 h incubation of films immersed in bacteria suspension in saline solution with added ascorbic acid (vitamin C; dark grey column) with or without US at start. (b) Live/dead imaging of NT ANN film with bacteria, solution of bacteria near the film and clear bacteria for *S. epidermidis* test in saline suspension.

**Influence on membrane compactness.** The fraction of dead bacteria obtained after US stimulation with the NT ANN films was also detected and visualized using the live/dead test. Fig. 8(b) shows the live/dead fraction of bacteria detected in case of *S. epidermidis*. The film itself adsorbed the dye mixture, which strongly limited the ability to detect the bacteria directly on the film. However, we were able to clearly detect bacteria in the saline medium above the film. Consequently, the intensive staining with propidium iodine (PI) showing red fluorescence indicates a very large fraction of dead bacteria.

The morphological characteristics of the bacterial cells attached to the film after testing in saline suspension were investigated using SEM microscopy. For this, the bacteria detected on the piezoelectric NT ANN films were compared with the bacteria on the NT as-prepared films with US stimulation. This study was performed using both Gram-negative *E. coli* and Gram-positive *S. epidermidis* bacteria. In both cases, we observed a damaged bacterial cell envelope when the bacteria were in contact with the piezoelectric NT ANN tubes and lack of morphological damage for the bacteria detected on the NT as-prepared film (Fig. 9(a and b)), confirming that the observed bacteriocidal effect for the NT ANN film in saline suspension in the antibacterial assay. Smith *et al.* showed that charge is present along the full length of each PLLA tube bent at the surface of NT films and that the top of the bent tubes holds a positive charge.<sup>22</sup> Accordingly, the whole presented surface of the ANN sample should have an effect on bacteria. We observed a lot of residual bacterial cells after complete damage of the cell structure (small dots on the tubes (Fig. 9(a)) observed for *E. coli*) and damaged cell envelope for *S. epidermidis* (Fig. 9(b)). This indicates that the long *E. coli*

bacterial cells in contact with the top of the tubes were intensively ruptured and disintegrated. Some of them that were aligned with the tube length maintained their compactness, however, membrane distortion was observed. For the shorter *S. epidermidis* bacteria, cell rupture did not occur; however, clear membrane distortion was observed. Similar membrane distortions were observed by Ando *et al.*, who showed a clear difference in bacterial cell surface morphology when their death was caused by piezoelectricity or with another stimuli (including heat, drying, or pH).<sup>8</sup> We also observed that US stimulation did not affect the orientation of the annealed PLLA tubes, which remained in the island formation as that at the before treatment. In contrast, sonication significantly changed the orientation of the tubes in the as-prepared films (Fig. 9(a and b) right and ESI S7 (Fig. S11†)). Due to their lower crystallinity, they were more elastic. Although the annealed and non-annealed NT PLLA films were detected to have a similar piezo-degradation potential (Fig. 7), the difference in their topography after US stimulation indicates that the annealed tubes were more stable and less mobile. Consequently, it is easier for bacteria to mechanically deform them just by landing on their surface, resulting in the generation of a piezo-signal and leading to the antibacterial effect observed even without US stimulation. Due to the movement of the tubes under US stimulation, a similar damaging effect was not detected on the NT as-prepared films when tested in suspension.

After 24 h of incubation of the immersed NT ANN film in *E. coli* saline solution, the membrane damage was optically observed using stain colours (FM 4-64 and DAPI) and a confocal microscope. Closer observation showed an intact membrane (red) for *E. coli* bacteria after incubation in saline solu-





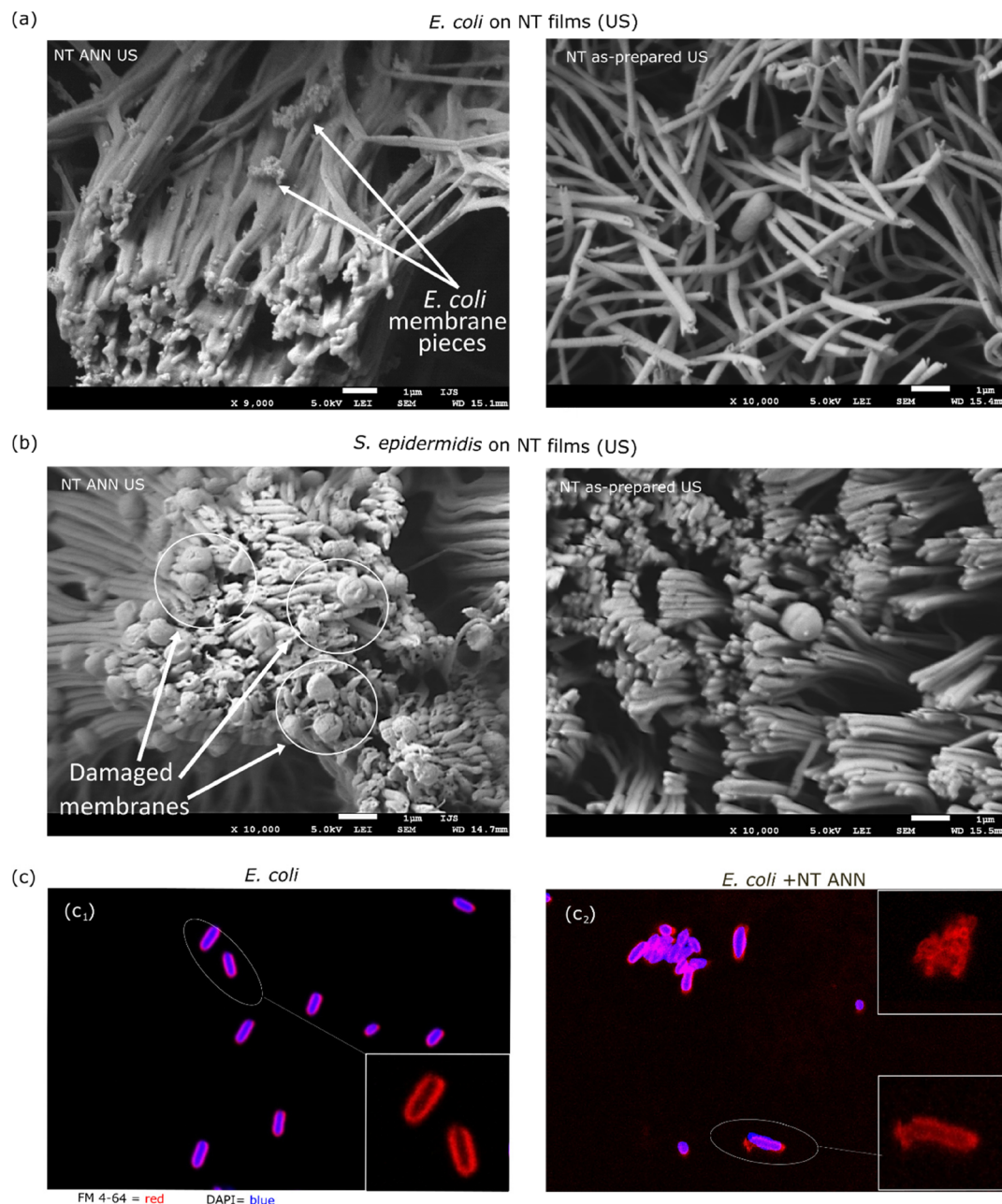


**Fig. 9** SEM images of (a) *E. coli* and (b) *S. epidermidis* bacteria on the nanotextured film surfaces after US stimulation for 30 min following 24 h incubation in saline suspension after cell fixation for NT ANN sample (left) and NT as-prepared sample. (c) FM 4-64 (red) and DAPI (blue) staining of *E. coli* bacteria (c<sub>1</sub>) and bacteria in contact with NT ANN film (c<sub>2</sub>) after test in saline solution with US stimulation.

tion and US (Fig. 9(c<sub>1</sub>)). However, for the bacteria in contact with the NT ANN film, an uneven distribution of the staining, indicating membrane damage, and rupture of the membrane were observed (Fig. 9(c<sub>2</sub>)). Also, the observed agglomeration of bacteria indicated their death.

The bacteriocidal effect was confirmed for the NT ANN sample with or without US stimulation as a result of the detected piezoelectric properties of the sample in combination with the nanotextured topography, which allows better mechanical deformation using US and more available surface.

Under mechanical stimulation, we presume that a positive charge is present on the surface and responsible for membrane damage in bacteria, leading to their death *via* only the contact-kill mechanism. Similar membrane damage and disruption of the transmembrane potential due to the exchange of cationic ions on the cell membrane and positively charged polymer surface was observed for positively charged quaternary ammonium compounds and proposed as the mechanism for bacteria death.<sup>16</sup> A positive charge can generate an electric field with the adhered bacteria, resulting in the removal of



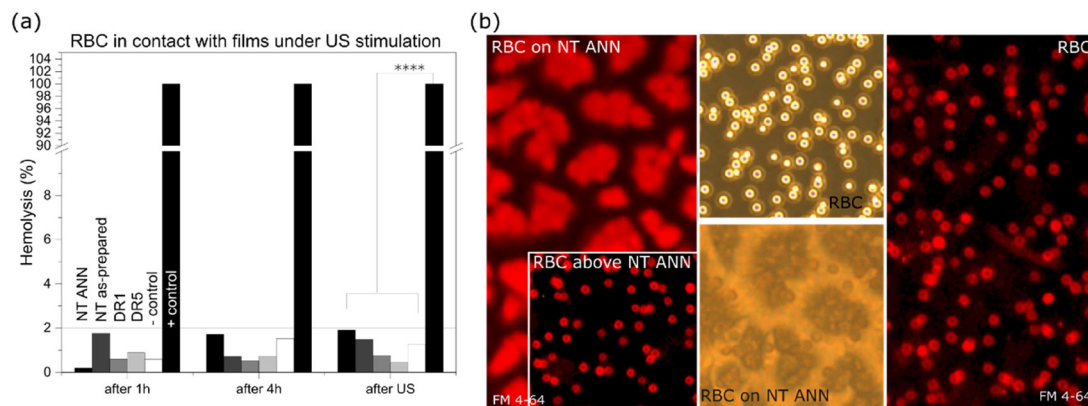


**Fig. 10** Piezo-stimulation effect in red blood cells (RBC). (a) Test of hemolysis for films (nanotextured annealed (NT ANN), NT as-prepared, drawn (DR5) and undrawn film (DR1)) in contact with RBCs compared to + and – control (damaged RBC in water and undamaged RBC in HEPES medium, respectively) using US stimulation: 30 min, 80 kHz, 30% power and (b) FM 4-64 red staining of RBC membranes and optical pictures of RBC in contact with nanotextured annealed film (RBC + NT ANN) after US stimulation compared to intact RBC reference in HEPES.

their membrane lipids and the dramatic electron loss, causing a distortion in their cell shape and leading to cell death.<sup>16,17</sup> We believe that poor contact is the reason for the low antibacterial properties of the NT ANN film when tested in the growth medium (50% lower OD value for *E. coli* bacteria) as a result of the contact-kill mechanism alone. According to the proposed mechanism, our films can be considered as an alternative to the established antibacterial therapies given that electric stimulation can prevent the emergence of bacteria resistance.<sup>1</sup>

### Hemolysis test and RBC membrane compactness

The effect of piezoelectricity was also investigated to determine if it damages red blood cells (RBC) through absorbance measurements of released hemoglobin (540 nm) and membrane staining. Less than 2% of released hemoglobin was detected after the films were in contact with RBC for 4 h for all the films with US stimulation (80 kHz, 30% power; Fig. 10(a)) and without US (ESI S8 (Fig. S12 and S13†)), compared to the positive control with RBC incubated in water. Disc-shaped RBC were detected both directly on the film surface and in the medium above the films (based on brightfield images in Fig. 10(b)). The potential damage in the RBC membranes was checked with the same FM 4-64 staining used for staining the bacterial membranes. Staining resulted in red fluorescence in membranes without penetration of the dye inside the cells, confirming their compactness and absence of any mechanical damage (Fig. 10(b)). Using full power at 80 kHz US, 40%–90% damage to the RBC was observed (ESI S8 (Fig. S12†)) for all the films with a nanotextured surface. The effect was the most pronounced for the non-piezoelectric NT films (90% for NT P(DL) LA), which led to the conclusion that it was caused by the topographical effect. In contrast, this effect was not detected for the drawn films.

The bactericidal effect on the surface of the NT ANN films was observed after the bacteria landed on their surface (without US stimulation, Fig. 6) or if the films were additionally deformed in ultrasound (with US stimulation, Fig. 6). In

this case, it can be concluded that for a suitable dose of ultrasonic deformation, piezo-stimulation with the use of fully organic polymers can be optimized. A wide range of mechanical deformations capable of inducing a piezoelectric response is needed for achieving an antimicrobial effect, and therefore a useful tool for attaining the required selectivity. Selective interactions with bacterial and mammalian cells are ultimately necessary for optimizing piezo-stimulation as a therapeutically applicable antimicrobial approach, which is highly efficient against bacteria and compatible with mammalian cells. Electric stimulation is also beneficial for mammalian cells,<sup>45,46</sup> and therefore the prepared biodegradable films with antibacterial properties can be applicable to increase cell proliferation, migration and differentiation for wound healing or tissue regeneration and preventing infections associated with chronic wounds. The main benefits of its application in infection control are expected from the non-specificity of the piezo-stimulation mechanism used to damage bacteria. This mechanism applies physical deformation, which does not leave them too many options to adopt and develop a resistance mechanism, as is the case with most of the currently used antimicrobial technologies.

## Conclusion

Fully organic, biodegradable, polymeric films were designed as PLLA piezoelectrics with nanotextured or smooth surfaces. Nanotexturing combined with post-processing annealing resulted in a higher specific surface area and better crystallinity, which jointly affected their piezo-degradation potential, implying a significant improvement in their piezoelectric properties. Piezostimulation induced bacterial death in both Gram-positive and Gram-negative bacterial strains. The films were not capable of producing ROS and the antimicrobial effect on their surface was achieved even in the presence of an ROS scavenger. Either bacterial cells landing on their surface



or application of US stimulation, which caused mechanical deformation of the nanotextured PLLA piezoelectric films, generated a surface charge, affecting the bacterial membrane. In the case of the non-piezoelectric films, the long and flexible pillars on the nanotextured films could not cause an antimicrobial effect just by nanotexturing. Therefore, the detected damage in the cell bacterial membrane was due to the disrupted transmembrane potential, leading to cell death with time (>5 h). Due to the poor adhesion of the bacterial cells to the surface of the films, the effect was not fast. Further improvement in their efficacy is expected using adhesion molecules, which will enhance the bacterial attachment to the surface of the films, which we consider an interesting and potential option to be explored in the future. After optimization of the conditions of mechanical stimulation, high usability of these films for therapeutic use is expected.

## Author contributions

Research conceptualization, L. G. and M. V.; fluorescence confocal microscope observations, M. P. N.; data curation, L. G., M. P. N. and M. V.; writing – original draft preparation, L.G.; writing – review and editing, M. P. N., M. V. and M. S.; visualization, L. G. and M. V.; supervision, M. V.; funding acquisition, M. V., M. S.

## Conflicts of interest

The authors declare no conflict of interest. The funders had no role in the design of the study; in the collection, analyses, or interpretation of data; in the writing of the manuscript, or in the decision to publish the result.

## Acknowledgements

The authors are grateful to Dr Urška Gabor, Msc. Damjan Vengust and David Fabian from Advanced Materials Department, IJS, for help with performing XRD, Raman and piezoelectric measurements.

The work has been funded by the Slovenian Research Agency (ARRS) within grants J2-8169, N2-0150 and PR-08338 and research programs P2-0091 and PR-0099.

## References

- 1 M. M. Fernandes, E. O. Carvalho and S. Lanceros-Mendez, Electroactive Smart Materials: Novel Tools for Tailoring Bacteria Behavior and Fight Antimicrobial Resistance, *Front. Bioeng. Biotechnol.*, 2019, **7**, 277.
- 2 C. Ribeiro, S. Moreira, V. Correia, V. Sencadas, J. G. Rocha, F. M. Gama, *et al.*, Enhanced proliferation of pre-osteoblastic cells by dynamic piezoelectric stimulation, *RSC Adv.*, 2012, **2**, 11504–11509.
- 3 H. Miyazaki, M. Kinoshita, A. Saito, T. Fujie, K. Kabata, E. Hara, *et al.*, An ultrathin poly(L-lactic acid) nanosheet as a burn wound dressing for protection against bacterial infection, *Wound Repair Regen.*, 2012, **20**, 573–579.
- 4 H. Guo, Z. Li, S. Dong, W. Chen, L. Deng, Y. Wang, *et al.*, Piezoelectric PU/PVDF electrospun scaffolds for wound healing applications, *Colloids Surf., B*, 2012, **96**, 29–36.
- 5 S. N. Gorodzhia, A. R. Muslimov, D. S. Syromotina, A. S. Timin, N. Y. Tevetkov, K. V. Lepik, *et al.*, A comparison study between electrospun polycaprolactone and piezoelectric poly(3-hydroxybutyrate-co-3-hydroxyvalerate) scaffolds for bone tissue engineering, *Colloids Surf., B*, 2017, **160**, 48–59.
- 6 S. Guerin, S. A. M. Tofail and D. Thompson, Organic piezoelectric materials: milestones and potential, *NPG Asia Mater.*, 2019, **10**.
- 7 M. Ando, S. Takeshima, Y. Ishiura, K. Ando and O. Onishi, Piezoelectric antibacterial fabric comprised of poly(l-lactic acid) yarn, *Jpn. J. Appl. Phys.*, 2017, **56**, 10PG01.
- 8 M. Ando, D. Tamakura, T. Inoue, K. Takumi, T. Yamanaga, R. Todo, *et al.*, Electric antibacterial effect of piezoelectric poly(lactic acid) fabric, *Jpn. J. Appl. Phys.*, 2019, SLLD09.
- 9 T. Wang, H. Chen, C. Yu and X. Xie, Rapid determination of the electroporation threshold for bacteria inactivation using a lab-on-a-chip platform, *Environ. Int.*, 2019, **132**(April), 105040.
- 10 E. O. Carvalho, M. M. Fernandes, J. Padrao, A. Nicolau, J. Marques-Marchan, A. Asenjo, *et al.*, Tailoring Bacteria Response by Piezoelectric Stimulation, *ACS Appl. Mater. Interfaces*, 2019, **11**(30), 27297–27305.
- 11 S. Kumar, R. Vaish and S. Powar, Surface-selective bactericidal effect of poled ferroelectric materials, *J. Appl. Phys.*, 2018, **124**, 014901.
- 12 G. Tan, S. Wang, Y. Zhu, L. Zhou, P. Yu, X. Wang, *et al.*, Surface-Selective Preferential Production of Reactive Oxygen Species on Piezoelectric Ceramics for Bacterial Killing, *ACS Appl. Mater. Interfaces*, 2016, **8**(37), 24306–24309.
- 13 I. S. Vatlin, R. V. Chernozem, A. S. Timin, A. P. Chernova, E. V. Plotnikov, Y. R. Mukhortova, *et al.*, Bacteriostatic Effect of Piezoelectric Poly-3-Hydroxybutyrate and Polyvinylidene Fluoride Polymer Films under Ultrasound Treatment, *Polymers*, 2020, **12**, 240.
- 14 D. V. Bayramol, N. Soin, A. Dubey, R. Kant, R. Priyadarshini, S. S. Roy, *et al.*, Evaluating the fabric performance and antibacterial properties of 3-D piezoelectric spacer fabric, *J. Text. Inst.*, 2018, **5000**, 1–7.
- 15 Y. Wang, Y. Xu, S. Dong, P. Wang, W. Chen, Z. Lu, *et al.*, Ultrasonic activation of inert poly(tetrafluoroethylene) enables piezocatalytic generation of reactive oxygen species, *Nat. Commun.*, 2021, **12**(3508), 1–8.
- 16 R. Kaur and S. Liu, Antibacterial surface design – Contact kill, *Prog. Surf. Sci.*, 2016, **91**(3), 136–153.
- 17 G. Wang, H. Feng, L. Hu, W. Jin, Q. Hao, A. Gao, *et al.*, An antibacterial platform based on capacitive carbon-doped





- TiO<sub>2</sub> nanotubes after direct or alternating current charging, *Nat. Commun.*, 2018, **9**(2055), 1613–1619.
- 18 E. P. Ivanova, J. Hasan, H. K. Webb, V. K. Truong, G. S. Watson, J. A. Watson, *et al.*, Natural Bactericidal Surfaces: Mechanical Rupture of *Pseudomonas aeruginosa* Cells by Cicada Wings, *Small*, 2012, **8**(16), 2489–2494.
  - 19 A. Jaggesar, H. Shahali, A. Mathew and P. K. D. V. Yarlagadda, Bio-mimicking nano and micro-structured surface fabrication for antibacterial properties in medical implants, *J. Nanobiotechnol.*, 2017, **15**, 64.
  - 20 M. N. Dickson, E. I. Liang, L. A. Rodriguez, N. Vollereaux and A. F. Yee, Nanopatterned polymer surfaces with bactericidal properties, *Biointerphases*, 2015, **10**(2), 021010.
  - 21 Y. Jang, W. T. Choi, C. T. Johnson, A. J. Garcia, P. M. Singh, V. Breedveld, *et al.*, Inhibition of Bacterial Adhesion on Nanotextured Stainless Steel 316L by Electrochemical Etching, *ACS Biomater. Sci. Eng.*, 2018, **4**, 90–97.
  - 22 M. Smith, T. Chalklen, C. Lindackers, Y. Calahorra, C. Howe, A. Tamboli, *et al.*, Poly-L-Lactic Acid Nanotubes as Soft Piezoelectric Interfaces for Biology: Controlling Cell Attachment via Polymer Crystallinity, *ACS Appl. Bio Mater.*, 2020, **3**, 2140–2149.
  - 23 L. Udovc, M. Spreitzer and M. Vukomanovic, Towards hydrophilic piezoelectric poly-L-lactide films: optimal processing, post-heat treatment and alkaline etching, *Polym. J.*, 2020, **52**, 299–311.
  - 24 M. Smith, C. Lindackers, K. McCarthy and S. Kar-narayan, Enhanced Molecular Alignment in Poly-L-Lactic Acid Nanotubes Induced via Melt-Press Template-Wetting, *Macromol. Mater. Eng.*, 2019, **304**, 1800607.
  - 25 S. Farah, D. G. Anderson and R. Langer, Physical and mechanical properties of PLA, and their functions in widespread applications—A comprehensive review, *Adv. Drug Delivery Rev.*, 2016, **107**, 367–392.
  - 26 ISO 21702 : 2019- Measurement of antiviral activity on plastics and other non-porous surfaces.
  - 27 E. Pinho, L. Magalhães, M. Henriques and R. Oliveira, Antimicrobial activity assessment of textiles: standard methods comparison, *494 Ann. Microbiol.*, 2011, **61**, 493–498.
  - 28 C. S. Lovell, J. M. Fitz-Gerald and C. Park, Decoupling the effects of crystallinity and orientation on the shear piezoelectricity of polylactic acid, *J. Polym. Sci., Part B: Polym. Phys.*, 2011, **49**(21), 1555–1562.
  - 29 K. Takahashi, D. Sawai, T. Yokoyama, T. Kanamoto and S.-H. Hyon, Crystal transformation from the  $\alpha$ - to the  $\beta$ -form upon tensile drawing of poly(L-lactic acid), *Polymer*, 2004, **45**(14), 4969–4976.
  - 30 C. A. C. Erbetta, R. J. Alves, J. M. Resende, F. R. S. Freitas and R. G. de Sousa, Synthesis and Characterization of Poly (D,L-Lactide-co-Glycolide) Copolymer, *J. Biomater. Nanobiotechnol.*, 2012, **3**, 208–225.
  - 31 M. Smith, Y. Calahorra, Q. Jing, S. Kar-narayan, M. Smith, Y. Calahorra, *et al.*, Direct observation of shear piezoelectricity in poly-l-lactic acid nanowires, *APL Mater.*, 2017, **5**, 074105.
  - 32 M. Y. E. Yau, I. Gunkel, B. Hartmann-Azanza, W. Akram, Y. Wang, T. Thurn-Albrecht, *et al.*, Semicrystalline Block Copolymers in Rigid Confining Nanopores, *Macromolecules*, 2017, **50**, 8637–8646.
  - 33 A. Cafarelli, A. Marino, L. Vannozzi, J. Puigmartí-Luis, S. Pané, G. Ciofani, *et al.*, Piezoelectric Nanomaterials Activated by Ultrasound: The Pathway from Discovery to Future Clinical Adoption, *ACS Nano*, 2021, 11066–11086.
  - 34 S. S. Rashwan, I. Dincer and A. Mohany, Investigation of acoustic and geometric effects on the sonoreactor performance, *Ultrason. Sonochem.*, 2020, **68**, 105174.
  - 35 M. Hoop, X. Chen, A. Fer, F. Mushtaq, G. Ghazaryan, T. Tervoort, *et al.*, Ultrasound-mediated piezoelectric differentiation of neuron-like PC12 cells on PVDF membranes, *Sci. Rep.*, 2017, **7**(4028), 1–8.
  - 36 R. Das, E. J. Curry, T. T. Le, G. Awale, Y. Liu, S. Li, *et al.*, Nano Energy Biodegradable nanofiber bone-tissue scaffold as remotely-controlled and self-powering electrical stimulator, *Nano Energy*, 2020, **76**, 105028.
  - 37 L. I. Jinga, G. Popescu-pelin, G. Socol, S. Mocanu, M. Tudose, D. C. Culita, *et al.*, Chemical Degradation of Methylene Blue Dye Using TiO<sub>2</sub>/Au Nanoparticles, *Nanomaterials*, 2021, **11**(1605), 1–10.
  - 38 S. Liu, B. Jing, C. Nie, Z. Ao, X. Duan, B. Lai, *et al.*, Piezoelectric activation of peroxydisulfate by MoS<sub>2</sub> nanoflowers for the enhanced degradation of aqueous organic pollutants, *Environ. Sci.: Nano*, 2021, **8**, 784–794.
  - 39 C. Lei, L. Song and S. Zhang, Study on the piezoelectric catalytic degradation dyes performance of three-dimensional bismuth tungstate microflower, *Ceram. Int.*, 2020, **46**(18), 29344–29351.
  - 40 X. Xue, W. Zang, P. Deng, Q. Wang, L. Xing, Y. Zhang, *et al.*, Piezo-potential enhanced photocatalytic degradation of organic dye using ZnO nanowires, *Nano Energy*, 2015, **13**, 414–422.
  - 41 T. Hou, F. Cao, M. Li, J. Wang and L. Lv, Harvesting the Vibration Energy with BaTiO<sub>3</sub>@Graphene for the Piezocatalytic Degradation of Methylene Blue, *J. Environ. Sci. Eng. Technol.*, 2020, **8**, 84–91.
  - 42 M. Michalska, F. Gambacorta, R. Divan, I. S. Aranson, A. Sokolov, P. Noirot, *et al.*, Tuning antimicrobial properties of biomimetic nanopatterned surfaces, *Nanoscale*, 2018, **10**, 6639–6650.
  - 43 G. Moran and R. Meallet-Renault, Superhydrophobic Surfaces Toward Prevention of Biofilm-Associated Infections, in *Bacterial Pathogenesis and Antibacterial Control*, ed. S. Kirmusaoğlu, IntechOpen, London, 2018, pp. 95–109.
  - 44 L. Gazvoda, B. Višić, M. Spreitzer and M. Vukomanović, Hydrophilicity affecting the enzyme-driven degradation of piezoelectric poly-l-lactide films, *Polymers*, 2021, 1719.
  - 45 M. Rouabhia, H. Park, S. Meng, H. Derbali and Z. Zhang, Electrical stimulation promotes wound healing by enhancing dermal fibroblast activity and promoting myofibroblast transdifferentiation, *PLoS One*, 2013, e71660.
  - 46 M. R. Asadi and G. Torkaman, Bacterial Inhibition by Electrical Stimulation, *Adv. Wound Care*, 2014, **3**(2), 91–97.

